Analysis of the effects of arc-shape fibre structure on the performance of passively mode-locking thulium/holmium-doped fibre laser

HARITH AHMAD[1,2,*], KIRUBHASHNI LOGANATHAN[1], NORAZRIENA YUSOFF[3], MUHAMAD ZHARIF SAMION[1], KAVINTHERAN THAMBIRATNAM[4]
[1]*Photonics Research Centre, Universiti Malaya, 50603 Kuala Lumpur, Malaysia*
[2]*Adjunct Professor, Department of Physics, Faculty of Mathematics and Natural Sciences, Universitas Negeri Malang, Malang 65145, Indonesia*
[3]*Department of Physics, Faculty of Science, Universiti Malaya, 50603 Kuala Lumpur, Malaysia*
[4]*Physics Department, Kulliyyah of Science, International Islamic University Malaysia, Bandar Indera Makhota, 25200 Kuantan, Malaysia*

This study investigated the impact of arc-shaped fibre structures coated with a composite material on a Thulium/Holmium-doped fibre laser (THDF). Two types of arc-shaped fibres were utilised: single and dual arc. Both arc-shaped fibres were fabricated using the wheel-polishing technique. A two-step polishing process was employed for the dual arc-shaped fibre. The reduced graphene oxide/manganese oxide (rGO/Mn_3O_4) composite was subjected to hydrothermal treatment and then dropped onto both arc-shaped fibres. The modulation depth of rGO/Mn_3O_4 in a single arc-shaped fibre was 51.15% and 48.79% for the dual arc. Mode-locked pulses were generated individually by placing the saturable absorbers (SAs) in the cavity and fine-tuning the polarisation controller (PC). The pulse duration was 1.544 ps and 1.634 ps for the single and dual arc-shaped fibres. The two mode-locked pulses produced were remarkably stable, with a signal-to-noise ratio (SNR) exceeding 60 dB. Due to its lower insertion loss, the single arc shape fibre-based SA outperformed the dual arc in various aspects, including SNR, pulse duration, average power, and efficiency. The findings of this work provide a compelling alternative for generating ultrashort pulse lasers that are both compact in size and highly effective in performance.

(Received May 22, 2025; accepted December 2, 2025)

Keywords: Mode-locking, Saturable absorber, Single arc-shape fibre, Dual arc-shape fibre, Reduced graphene oxide/Magnesium oxide

1. Introduction

One of the most critical issues that needs to be addressed in laser technology is the generation of ultrashort pulses. It has garnered significant attention because it can be utilised in various fields, including telecommunications [1-3], biomedical imaging [4-6], material processing [7-9], and spectroscopy [10, 11]. To be more specific, mode-locked fibre lasers have proven to be the most successful in generating ultrashort pulses due to their excellent stability, compactness, and ease of integration [12]. When it comes to operating mode-locked fibre lasers, the saturable absorber, also referred to as the SA, is a crucial component. It does this by influencing the optical characteristics within the laser cavity, ultimately generating sub-picosecond and picosecond pulses.

Over the past few years, a wide range of Transition Metal Oxides (TMOs) have been utilised extensively in generating mode-lock and Q-switch pulses as SA materials. Zinc oxide [13], Titanium dioxide (TiO_2) [13], Iron oxide (Fe_2O_3) [14], Stannic oxide (SnO_2) [15], Holmium oxide (Ho_2O_3) [16], and Vanadium oxides (VO) [17] are some of the examples of compounds that fall into this group. Manganese oxide is a well-known and effective TMO in the field of supercapacitors. Reasons for this include its low cost, safety, environmental friendliness, and high power density [18]. Manganese oxide can have different crystallographic structures containing different oxidation states, such as MnO, MnO_2, Mn_2O_3, and Mn_3O_4 [19]. Mn_3O_4 is a p-type semiconductor with outstanding electrical conductivity and good chemical and thermal durability, among other crystal phases of manganese oxide [20]. Furthermore, its excellent cycle stability, structural flexibility, and spinel framework, which allows varied oxidation states, make it an appealing material for supercapacitor applications [21]. Furthermore, Mn_3O_4 can be used as a catalyst [22], in optoelectronic devices [23], for lithium-ion batteries [24], or as a gas sensor [25]. However, despite its potential applications in several fields, Mn_3O_4 has not been thoroughly investigated, particularly in nonlinear optics for producing mode-locked pulsed lasers.

Using rGO/Mn_3O_4 composite as an SA is an innovative and pioneering method in the domain of mode-locked fibre lasers. This study aims to investigate the potential of this composite material for mode-locking, generating ultrashort pulses. By leveraging the characteristics of rGO/Mn_3O_4, this work seeks to examine its optical properties and behaviour as an SA. It will

enhance the understanding of its usefulness in generating pulses and create new avenues for further research.

To the best of the author's knowledge, no research has been conducted that investigates explicitly the arc-shaped rGO/Mn_3O_4 as an SA. In this research, the effect of the arc-shaped configuration on ultrashort pulse generation using the rGO/Mn_3O_4 composite as an SA was evaluated. More specifically, the aim is to establish which technique, a single or dual arc shape, performs better, that is, which of these two options can offer a lower pulse duration while maintaining good stability and higher output power. Comparing the mode-locking parameters of fibre lasers integrated with single and dual arc-shaped fibres will provide critical insights into potential improvements to the configuration and operation of mode-locked fibre laser systems, thereby enhancing the efficiency and robustness of ultrashort pulse generation for various applications.

2. Experimental procedure

2.1. Synthesis and characterisation of rGO/Mn_3O_4

2.1.1. Synthesis of rGO/Mn_3O_4 by hydrothermal approach

Graphene oxide (GO) purchased from Graphene Supermarket was thermally reduced to obtain reduced graphene oxide (rGO). An amount of 2.65 g of manganese acetate was added to a 50 mL beaker containing 15 mL of ethanol and stirred for 15 minutes. Subsequently, 15 mL of distilled water was added to the manganese acetate solution, and stirring was continued for 15 minutes. The resulting solution was mixed with the GO solution and stirred using a magnetic stirrer for 60 minutes. Next, the solution was put into the autoclave lined with Teflon and heated in the oven for 7 hours at a temperature of 150°C. The resultant mixture was repeatedly rinsed with distilled water and ethanol. The slurry was then subjected to a drying process for 7 hours at 60°C. Subsequently, it was heated in a furnace at a temperature of 450°C for 2 hours. The dry black powder was then ground to a fine powder with a mortar and pestle.

2.1.2. Characterisation of rGO/Mn_3O_4

Fig. 1 (a) shows the composite's field-emission scanning electron microscope (FESEM) image, captured at an accelerating voltage of 2 kV with a magnification of 50,000×. The Mn_3O_4 particles, with diameters ranging from 0.016 μm to 0.25 μm, were scattered on the rGO sheets. The sample was further analysed using an energy-dispersive X-ray (EDX) spectroscope to determine its chemical and elemental composition. Fig. 1 (b) clearly shows that the sample consists of Carbon (C), Oxygen (O), and Manganese (Mn), with atomic percentages of 48.71%, 40.77%, and 10.52%, respectively. The elemental mapping in Fig. 1 (c) indicates that C, O, and Mn are the main components of the rGO/Mn_3O_4 composite. The absence of peak signals for other elements in the EDX spectrum suggests that the sample has a high purity level. The UV-Vis absorption spectrum of the rGO/Mn_3O_4 composite was taken at room temperature in the 200 to 400 nm range, as shown in Fig. 1 (d). Remarkably, two absorption peaks are detected at 227 nm and 263 nm. The absorption peak at 227 nm is due to Mn_3O_4 [26], whereas the absorption peak in the proximity of 263 nm is due to the π–π* transitions occurring in the aromatic C–C bonds of the rGO-based materials [27,28]. The results of these studies demonstrated a reduction in GO after hydrothermal treatment, providing evidence for the formation of the rGO/Mn_3O_4 composite.

2.2. Preparation and characterisation of rGO/Mn_3O_4-based SA

2.2.1. Fabrication of single and dual arc-shaped fibre deposited with rGO/Mn_3O_4

The arc-shaped fibres were fabricated using a wheel polisher to ensure a uniform surface polish. It was accomplished by wrapping sandpaper around a cylinder, completely covering the cladding area of the SMF-28 fibre. It caused a portion of the SMF-28 fibre's cladding to be removed, resulting in a new platform for interaction with the evanescent field [29]. The SMF-28 had one end attached to a tunable laser source and the other to an optical power meter, which continuously measured the insertion loss. Polishing was performed on the single arc-shaped fibre until an insertion loss of approximately 3.4 dB was obtained. For the dual arc-shaped fibre, polishing was continued until an estimated insertion loss of roughly 2.5 dB was achieved. A slight horizontal adjustment was made while retaining vertical alignment, and the operation was repeated for the second arc, resulting in an estimated insertion loss of about 2.5 dB. The dual arc-shaped fibre exhibited an insertion loss of around 5 dB. The prepared solution was drop-cast on the two arc-shaped fibres on a glass slide. Fig. 2 (a) and (b) show the microscopic images of the drop-casted single and dual arc-shaped fibres, respectively. A total of 2.5 μL was drop-casted in the single arc-shaped fibre, while in the case of the dual arc-shaped fibre, 2.5 μL were drop-casted in each arc, resulting in a total of 5 μL.

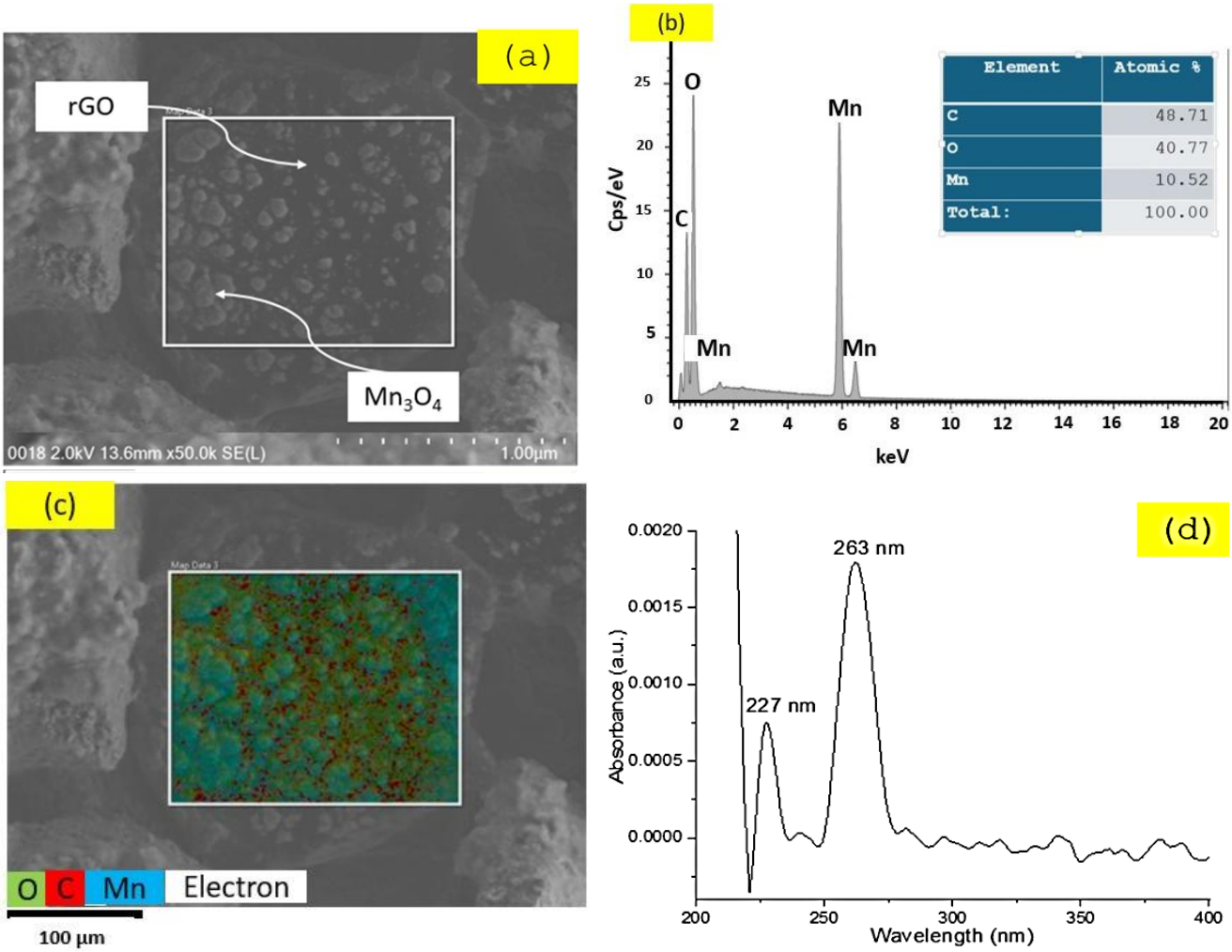

Fig. 1. The characterisation of rGO/Mn_3O_4 composite (a) FESEM image (b) EDX analysis (c) elemental mapping and (d) UV-Vis spectrum (colour online)

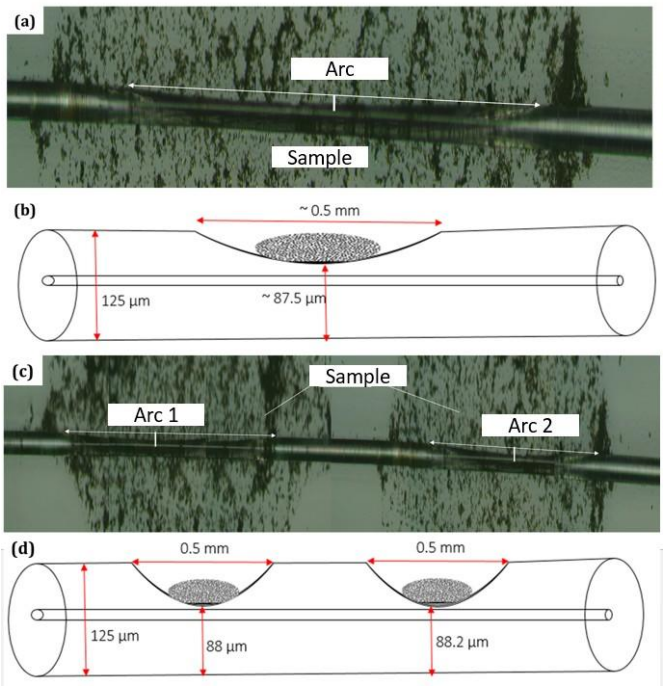

Fig. 2. a) Microscopic image of a single arc-shaped fibre, b) schematic diagram indicating the thickness of the arc-shaped fibre area covering the material, c) microscopic image of a dual arc-shaped fibre and d) schematic diagram indicating the thickness of the arc-shaped fibre with the material (colour online)

2.2.2. Optical nonlinearity of rGO/Mn_3O_4-based SA

The optical nonlinearity of the prepared SAs was measured using the twin detector approach, as shown in Fig. 3. The light source is a thulium-doped fibre laser (TDFL). The device used in this experiment features a mode-locked pulse with the following parameters: an 18.705 MHz repetition rate, a centre wavelength of 1969 nm, and a pulse duration of 1.02 ps. For the experiment, the TDFL was connected to an optical attenuator to adjust the intensity of the incoming signal. First, the signal passed through a bare single-mode fibre (SMF-28) and then to the SAs. The obtained readings were plotted as nonlinear curves for both SAs. Then, the modulation depths were obtained from the curves. For the rGO/Mn_3O_4 single arc-shaped fibre, a modulation depth of 51.15% was obtained, and for the rGO/Mn_3O_4 dual arc-shaped fibre, a value of 48.79% was obtained. Fig. 4 illustrates the fitting graph.

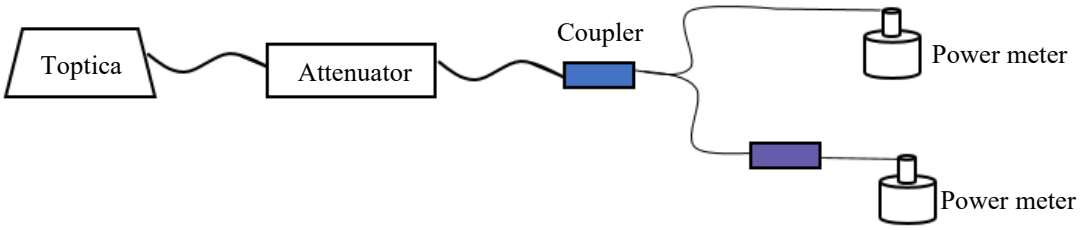

Fig. 3. Twin detection method

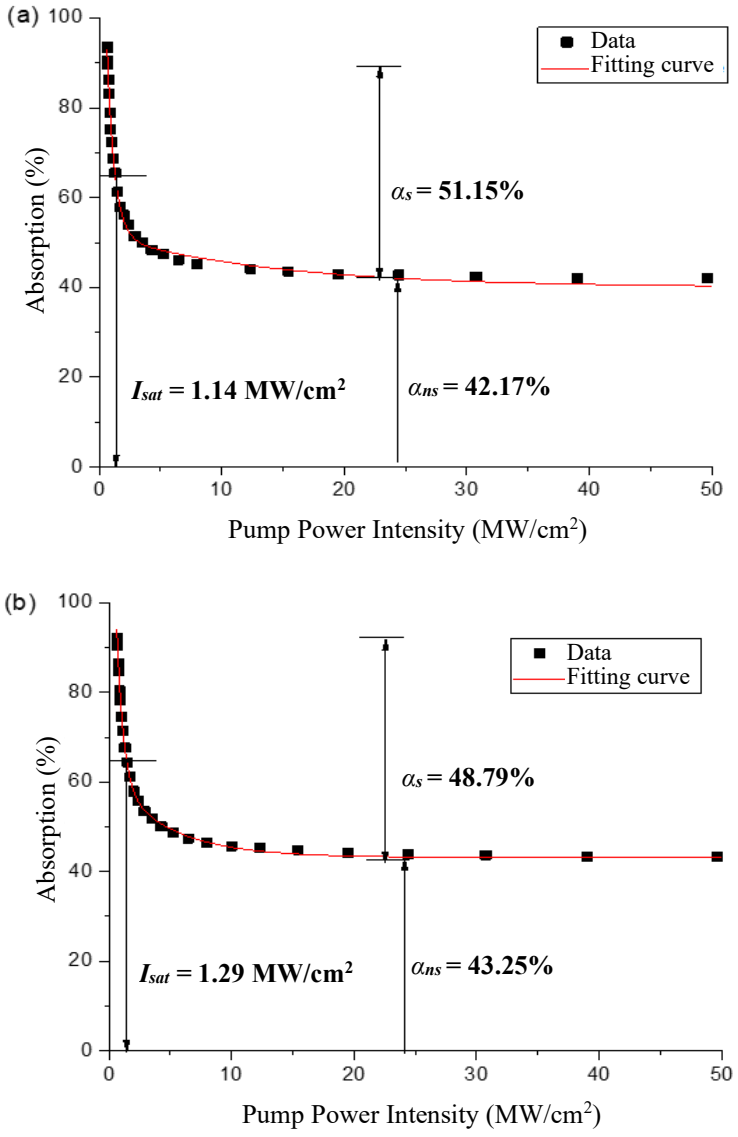

Fig. 4. Optical nonlinearity of rGO/Mn_3O_4 on (a) single arc-shape fibre and (b) dual arc-shape fibre

In Table 1, a comparison was made between the optical nonlinearity of rGO/Mn_3O_4 in single arc-shaped and dual arc-shaped fibres. According to the findings, rGO/Mn_3O_4 in a single arc-shaped fibre demonstrated a greater modulation depth and a lower saturation intensity than the dual arc-shaped fibre. A higher modulation depth leads to shorter pulses [30]. Additionally, a low saturation intensity is advantageous in SAs, as it can facilitate the achievement of a low threshold state in mode-locked lasers [31].

Table 1. Nonlinear absorption characterisation of rGO/Mn_3O_4 on a single and dual arc-shape fibre

Nonlinear absorption characterisation	rGO/Mn_3O_4 on a single arc-shaped fibre	rGO/Mn_3O_4 on a dual arc-shaped fibre
Modulation depth (%)	51.15	48.79
Non-saturable loss (%)	42.17	43.25
Saturation Intensity (MW/cm^2)	1.14	1.29

2.3. THDF laser cavity setup

Fig. 5 shows the setup for the THDF laser, where rGO/Mn_3O_4 drop-casted arc-shaped fibres were used as the SAs. Two laser diodes (LDs) generating at a wavelength of 1560 nm were utilised, along with two wavelength division multiplexers (WDMs) operating at 1560/2000 nm, to pump the 1.5 m THDF. Optical isolators were used at both ends of each LD to prevent any back reflections. A 90:10 cavity output coupler (OC) was included and connected to a 2000 nm ISO to ensure clockwise signal propagation. The 10% port was used for the signal analysis, and the remaining 90% was connected to the cavity. An OSA was used to get the optical spectrum of the pulse laser, and an optical power meter measured the output power. An oscilloscope and autocorrelator analysed the time-domain characteristics of the pulse. Finally, the arc-shaped fibre was placed after the polarisation controller (PC) to complete the cavity, ensuring a stable polarisation state.

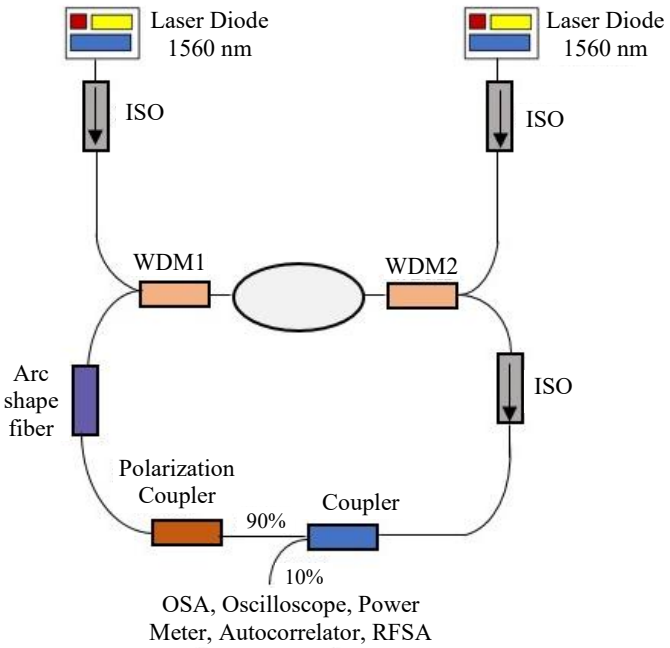

Fig. 5. Schematic representation of the THDF laser cavity (colour online)

3. Results and discussion

3.1. Passive mode locking of rGO/Mn_3O_4 on a single arc-shaped fibre

Mode-locking was demonstrated at a threshold pump power of 249.9 mW. The corresponding mode-locking characteristics of rGO/Mn_3O_4 are shown in Fig. 6 (a)–(e). Fig. 6(a) displays the mode-locking spectrum exhibiting Kelly's sidebands, with a bandwidth of 2.8 nm and a centre wavelength of 1895 nm, measured at a pump power of 274 mW. Fig. 6 (b) shows the autocorrelation (AC) trace of the mode-locked pulses, which is well matched with the $sech^2$ function, indicating a pulse duration of 1.544 ps. In addition, the RF spectrum of the mode-lock pulses was also measured, yielding a signal-to-noise ratio (SNR) of 65.3. (Fig. 6(c)). Fig. 6(d) shows the highest achievable output power of 1.18 mW when the pump power is at its maximum, with an efficiency of 0.56%. Fig. 6 (e) shows the laser output oscilloscope trace of the pulses, which repeat every 81.7 ns, resulting in a repetition rate of 12.24 MHz.

3.2. Passive mode locking of rGO/Mn_3O_4 on a dual arc-shaped fibre

Mode-locking was realised at a threshold pump power of about 253.5 mW. Fig. 7 (a)–(e) show the mode-locking results of rGO/Mn_3O_4 on a dual arc-shape fibre-based SA. Fig. 7 (a) shows the mode-locking spectrum with Kelly's sidebands, featuring a 3 dB bandwidth of 2.45 nm at a centre wavelength of 1895 nm, measured at a pump power

of 274 mW. Fig. 7(b) shows the AC trace of the mode-locked pulses, which is well-fitted by a sech² profile with a pulse duration of 1.634 ps. An SNR value of 63 dB was also measured, as shown in Fig. 7 (c). Fig. 7 (d) shows an efficiency of 0.39% and an output power of up to 0.83 mW. The train of pulses generated by mode-locking had a pulse-to-pulse spacing of 82.5 ns, corresponding to a fundamental frequency of 12.11 MHz, as illustrated in Fig. 7 (e).

Table 2 shows the findings for mode-locked fibre lasers with the two SAs. Both SAs generate mode-locked pulses at a centre wavelength of 1895 nm. Nevertheless, the performance of the generated mode-locked pulses using rGO/Mn_3O_4 on a single arc-shaped fibre-based SA is better than that of the counterpart using rGO/Mn_3O_4 on a dual arc-shaped fibre-based SA in terms of SNR, pulse duration, and efficiency. The pulse duration generated by rGO/Mn_3O_4 on a single arc-shape fibre-based SA is 1.544 ps, which is 5.66% shorter than the pulse generated by rGO/Mn_3O_4 on a dual arc-shape fibre-based SA. Moreover, the SNR and efficiency for rGO/Mn_3O_4 on a single arc-shaped fibre-based SA are 65.3 dB and 0.56%, respectively, which demonstrate higher characteristics compared to the values recorded when using rGO/Mn_3O_4 on a dual arc-shaped fibre-based SA. The repetition rate of rGO/Mn_3O_4 on a single arc-shaped fibre-based SA is slightly higher than that of rGO/Mn_3O_4 on a dual arc-shaped fibre-based SA. This minor difference could be due to the slight variation in the length of the arc-shaped fibre and also changes in the polarisation states.

To determine how close the pulses were to the transform limit, the time–bandwidth product (TBP) was calculated. While the spectral width $\Delta\lambda$ was taken from the optical spectrum and converted to frequency bandwidth $\Delta\nu \approx (c / \lambda_0^2)\,\Delta\lambda$, where λ_0. The centre wavelength and the pulse duration, Δt taken at the full width half maximum (FWHM) point, were measured using autocorrelation traces. After that, the TBP was computed as TBP = $\Delta t.\ \Delta\nu$. The TBP calculated for the single and dual arc-shaped fibre-based SAs were 0.361 and 0.334, respectively. These slightly higher values suggest the presence of residual chirp or dispersion.

The mode-locked fibre laser with a single arc-shaped SA performed better than the double arc-shaped one, primarily due to the higher insertion loss. The single arc-shape fibre exhibits a lower insertion loss of 3.4 dB compared to the dual arc-shape fibre, which has a total insertion loss of approximately 5 dB. A lower insertion loss, therefore, has resulted in better performance and stability of the laser system. The difference in laser performance between the two fibre configurations can also be attributed to the drop-casting process. In a single arc-shaped fibre, only one droplet of solution is cast on the fibre's surface, which does not interfere much with the fibre's optical properties. In the case of the dual arc-shaped fibre, having two droplets cast on the surface of the fibre may cause slightly higher scattering effects. Subsequently, excess absorption of the incident light by the SA material will reduce the fibre's ability to modulate the laser pulses effectively. As such, the dual arc-shape fibre will have a lower modulation depth and efficiency than the single arc-shape fibre. These effects might degrade the performance of the laser system. In addition, the shorter pulse duration of a single arc-shaped fibre is due to the SA's more significant modulation depth compared to the other one [32].

Table 2. Laser parameters generated by the two SAs

	rGO/Mn_3O_4 on a single arc-shaped fibre	**rGO/Mn_3O_4 on a dual arc-shape fibre**
Central wavelength (nm)	1895	1895
3 dB bandwidth (nm)	2.8	2.45
Pulse duration (ps)	1.544	1.634
SNR (dB)	65.3	63
Efficiency (%)	0.56	0.39
Repetition rate (MHz)	12.24	12.11
TBP	0.361	0.334

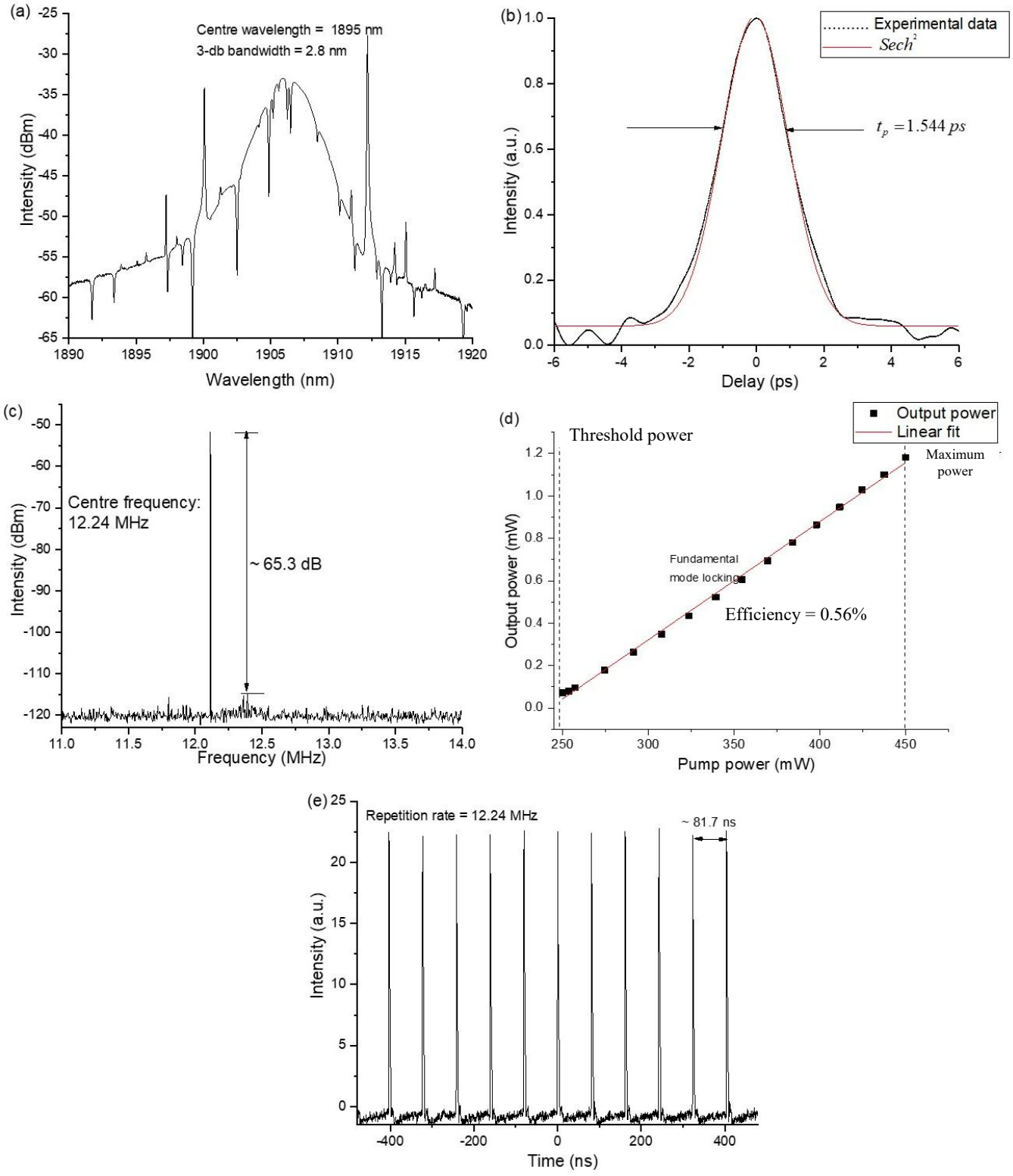

Fig. 6. Mode-locking characteristics of rGO/Mn_3O_4 on a single arc-shape fibre (a) OSA spectrum (b) autocorrelation (c) radio frequency spectrum (d) efficiency graph and (e) oscilloscope trace

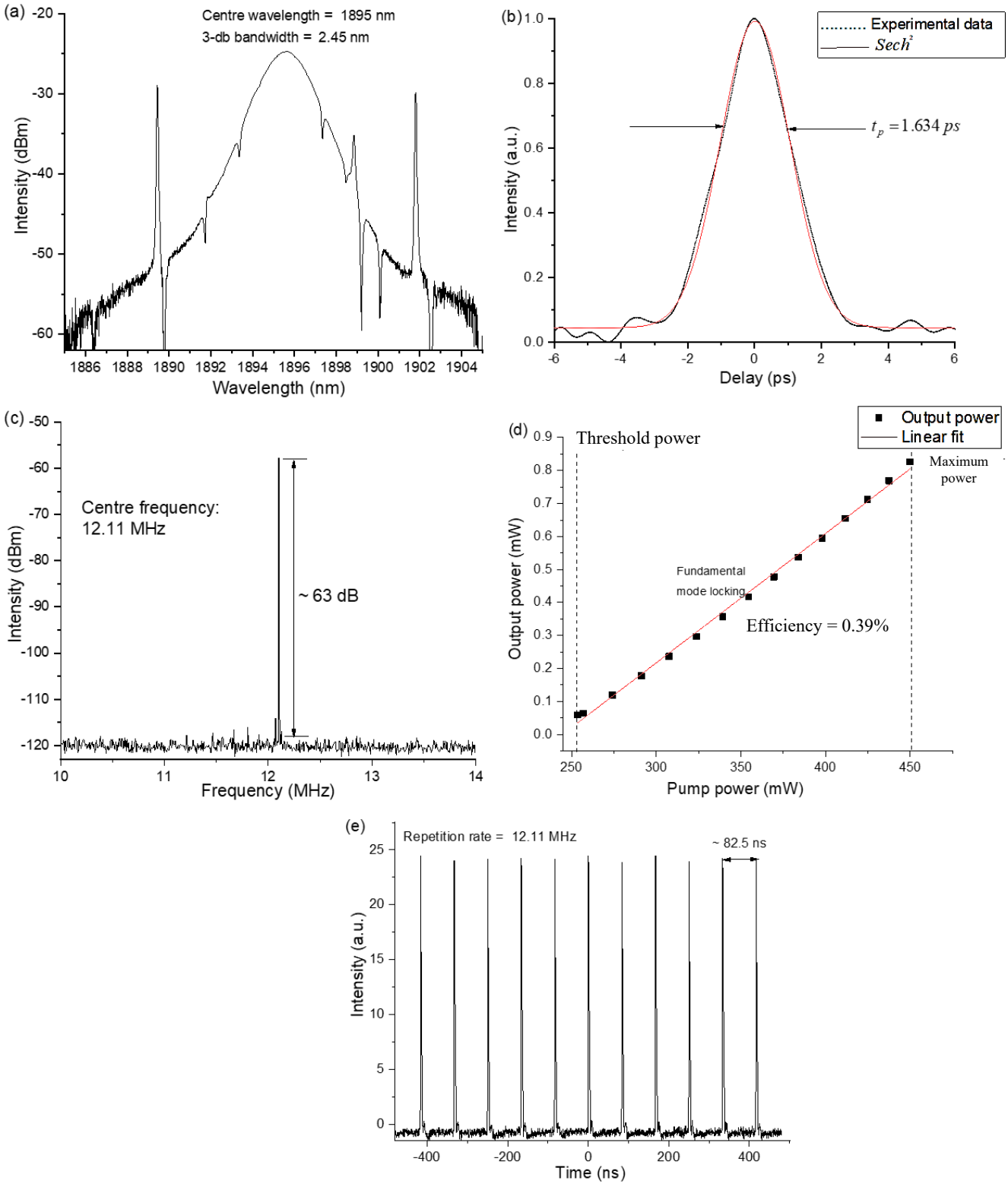

Fig. 7. Mode-locking characteristics of rGO/Mn_3O_4 on a dual arc-shape fibre (a) OSA spectrum (b) autocorrelation (c) radio frequency spectrum (d) efficiency graph and (e) oscilloscope trace

4. Conclusion

This study demonstrates the use of hydrothermal methods for effectively fabricating rGO/Mn_3O_4. The synthesised material was used as a mode-locking device to generate ultrashort pulses within the wavelength region of 1.9 µm. The study investigates the effect of rGO/Mn_3O_4 composites on the performance of single and dual arc-shaped fibres as laser modulators. Overall, it can be inferred that the laser performance is superior when

rGO/Mn_3O_4 is employed in a single arc-shaped fibre compared to a dual arc-shaped fibre. Shorter pulse duration, higher SNR, and better efficiency are evidence. The pulse durations for the single and dual arc-shaped optical fibres were 1.544 ps and 1.634 ps, respectively. The structural configuration of arc-shaped fibres is crucial for mode-locking, making it a significant element in fibre laser performance. These findings will aid in optimising the construction of the SA to enhance the mode-locking performance of fibre laser systems.

Acknowledgement

We thank Universiti Malaya for their funding under the IIRG001A-2023 grant.

References

[1] A. A. Krylov, S. G. Sazonkin, A. F. Kosolapov, A. D. Pryamikov, A. N. Kolyadin, I. A. Bufetov, Quantum Electron. **48**(7), 589 (2018).
[2] W. H. Knox, IEEE J. of Selected Topics in Quantum Electron. **6**(6), 1273 (2000).
[3] M. Wollenhaupt, A. Assion, T. Baumert, Springer Handbook of Lasers and Optics, Springer, Berlin, Heidelberg, 1047-1094 (2012).
[4] L. T. Schelhas, J. C. Shane, M. Dantus, Nanomedicine: Nanotechnology, Biology and Medicine **2**(3), 177 (2006).
[5] J. M. D. Cruz, V. V. Lozovoy, M. Dantus, J Photoch Photobio A **180**(3), 307 (2006).
[6] M. Sanchez, D. Gallego, H. Lamela, Opt. Express **30**(25), 44954 (2022).
[7] J. Bliedtner, C. Schindler, M. Seiler, S. Wächter, M. Friedrich, J. Giesecke, Laser Technik Journal **13**(5), 46 (2016).
[8] B. Voisiat, D. Gaponov, P. Gečys, L. Lavoute, M. Silva, A. Hideur, N. Ducros, G. Račiukaitis, Laser Applications in Microelectronic and Optoelectronic Manufacturing (LAMOM) XX, San Francisco, California, USA, **9350**, 120-127 (2015).
[9] G. Račiukaitis, IEEE J. Sel. Top Quant. **27**(6), 1 (2021).
[10] T. Kobayashi, Photonics **5** (3), 19 (2018).
[11] H. Pires, M. Baudisch, D. Sanchez, M. Hemmer, J. Biegert, Prog. Quant. Electron. **43**, 1 (2015).
[12] H. Chen, X. Jiang, S. Xu, H. Zhang, Chinese Optics Letters **18**(4), 041405 (2020).
[13] N. A. M. Muhammad, N. A. Awang, H. Basri, Optik **283**, 170855 (2023).
[14] D. Mao, X. Cui, Z. He, H. Lu, W. Zhang, L. Wang, Q. Zhuang, S. Hua, T. Mei, J. Zhao, Nanoscale **10**(45), 21219 (2018).
[15] L. Zhang, F. Wang, Opt. Fiber Technol. **80**, 103469 (2023).
[16] A. S. Al-Hiti, M. F. A. Rahman, S. W. Harun, P. Yupapin, M. Yasin, Opt. Fiber Technol. **52**, 101996 (2019).
[17] M. Rahman, M. M. Rusdi, S. W. Harun, M. Yasin, Nonlinear Opt., Quantum Opt. **48** (4), 295 (2018).
[18] N. Horti, A. Samage, M. A. Halakarni, S. Chavan, S. Inamdar, M. Kamatagi, S. Nataraj, Mater. Chem. Phys. **318**, 129276 (2024).
[19] H. Xia, Y. Wan, F. Yan, L. Lu, Mater. Chem. Phys. **143**(2), 720 (2014).
[20] B. Şahin, R. Aydin, H. Cetin, Superlattices and Microstructures **143**, 106546 (2020).
[21] M. Gao, J. Hu, B. Zhao, Z. Liu, J. Appl. Electrochem. **50**, 767 (2020).
[22] A. Askarinejad, M. Bagherzadeh, A. Morsali, Appl. Surf. Sci. **256** (22), 6678 (2010).
[23] H. S. Kim, H. G. Na, J. C. Yang, J. H. Jung, Y. S. Koo, N. J. Hur, H. W. Kim, J. Solid State Chem. **183** (10), 2445 (2010).
[24] Y. T. Lee, C. T. Kuo, T. R. Yew, ACS Appl. Mater. Inter. **13**(1), 570 (2020).
[25] L. Bigiani, C. Maccato, G. Carraro, A. Gasparotto, C. Sada, E. Comini, D. Barreca, ACS Applied Nano Materials **1**(6), 2962 (2018).
[26] M. R. Shaik, R. Syed, S. F. Adil, M. Kuniyil, M. Khan, M. S. Alqahtani, J. P. Shaik, M. R. H. Siddiqui, A. Al-Warthan, M. A. Sharaf, Saudi J. Biol. Sci. **28**(2), 1196 (2021).
[27] A. W. Rokmana, A. Asriani, H. Suhendar, K. Triyana, A. Kusumaatmaja, I. Santoso, Journal of Phyisics: Conference Series, IOP Publishing **1011**(1), 012007 (2018).
[28] W. Wang, O. O. Kapitanova, P. Ilanchezhiyan, S. Xi, G. N. Panin, D. Fu, T. W. Kang, RSC Advances **8**(5), 2410 (2018).
[29] H. Ahmad, K. Loganathan, N. Yusoff, Opt. Laser Technol. **166**, 109687 (2023).
[30] I. Jung, F. Kärtner, N. Matuschek, D. Sutter, F. Morier- Genoud, Z. Shi, V. Scheuer, M. Tilsch, T. Tschudi, U. Keller, Appl. Phys. B-Lasers O **65**(2), 137 (1997).
[31] K. Lau, N. Z. Abidin, M. A. Bakar, A. Latif, F. Muhammad, N. Huang, M. Omar, M. Mahdi, J. of Phys. Commun. **2**(7), 075005 (2018).
[32] L. Cheng, Y. Yuan, C. Liu, X. Cao, J. Su, X. Zhang, H. Zhang, H. Zhao, M. Xu, J. Li, Results in Physics **13**, 102282 (2019).

*Corresponding author: harith@um.edu.my